AFFINE COMPENSATION OF ILLUMINATION IN HYPERSPECTRAL REMOTE SENSING IMAGES

Pedro Latorre Carmona[(a)], Jose E. Moreno[(b)], Filiberto Pla[(a)], and Crystal B. Schaaf[(c)]

[(a)]Institute for New Imaging Technologies and Departamento de Lenguajes y Sistemas Informáticos, Universidad Jaume I, Castellon de la Plana, Spain

[(b)]Departamento de Física de la Tierra y Termodinámica, Universidad de Valencia, Valencia, Spain

[(c)]Department of Geography and Environment, Center for Remote Sensing, Boston University, Boston, USA

ABSTRACT

A problem when working with optical satellite or airborne images is the need to compensate for changes in the illumination conditions at the time of acquisition. This is particularly critical when working with time series of data. Atmospheric correction strategies based on radiative transfer codes may provide a rigorous solution but it may not be the best solution for situations where a huge amount of hyperspectral images may need to be processed and computational time is a critical factor. The GMES ("Global Monitoring for Environment and Security") initiative has promoted the creation of a new generation of satellites (the SENTINEL series) with "ultra-high resolution" and "superspectral imaging" capabilities [1]. Therefore, there is an urgent need to quickly and reliably compensate for changes in the atmospheric transmittance and varying solar illumination conditions. In this paper three different forms of affine transformation models (general, particular and diagonal) are considered as candidates for rapid compensation of illumination variations. They are tested on a series of simulated multispectral images of Top-Of-Atmosphere (TOA) radiance, where the surface is a synthetic scene of a test site in Spain called Barrax, where reference data for validation is available. The results indicate that in 2 of the more moderate Sun positions, for all the Visibilities tested, the particular affine method is better than the other 2. The results also indicate that the proposed methodology is satisfactory for practical normalization of varying illumination and atmospheric conditions in remotely sensed images required for operational or time critical applications.

Index Terms— Affine, illumination compensation, hyperspectral

1. INFLUENCE OF THE ATMOSPHERE AND APPLICATION OF THE $6S$ CODE

Sensors on remote sensing satellites measure the radiation reflected by the atmosphere-Earth coupled system illuminated by the sun. In the ideal case, the solar radiation would hit the surface and be reflected back to space. Therefore, the radiance would only be affected in this case by the reflectance (characteristics) of the surface. In the actual case, the signal is modified by the atmosphere. The $6S$ code (Second Simulation of the Satellite Signal in the Solar Spectrum) [2] allows the simulation of the interaction of light with the atmosphere and the surface on the Sun-Target-Sensor path.

Considering that the surface (or region) is Lambertian, which means that the reflected radiance is *isotropic*, and therefore it has the same value for (θ_r, ϕ_r), i. e., Zenith and Azimuth angles of the reflected radiance, and assuming a $6S$ type formulation that decouples gaseous absorptions from scattering events, the *simulated radiance* arriving at the satellite at the Top-Of-Atmosphere (TOA) can be written as:

$$L^{sim}(\mu_s, \mu_v, \phi) = t_g \cdot \left[L_0 + \frac{\mu_s E_{sc}}{\pi} \cdot \frac{T\uparrow T\downarrow \rho_s}{1 - S \cdot \rho_s} \right] = L_{path} + L_{surf}, \quad (1)$$

where t_g is the transmittance due to gases, L_0 is the intrinsic atmospheric radiance (or atmospheric path radiance), ρ_s is the surface reflectance, *S* is the *Spherical Albedo*, μ_s is the cosine of the *Solar Zenith Angle* and μ_v the cosine of the view zenith angle. ϕ is the relative azimuth between the Sun and viewing directions, E_{sc} is the *Extraterrestrial Solar Irradiance*, and $T\uparrow$ and $T\downarrow$ are, respectively, the upward and downward total atmospheric transmittances (for diffuse plus direct radiation) in the illumination and observation directions.

2. AFFINE TRANSFORMATION ESTIMATION FOR ILLUMINATION CHANGES

We use a vector $l \in R_+^D$ to denote a measurement from a D bands multispectral sensor, which can be a camera or a system in a satellite. We also assume a linear behaviour of the sensor (at least in the spectral region of interest) and therefore the application of a transformation model is valid whether we consider l as the *radiance* reaching the sensor, or the response of this sensor. Under a change in the illumination characteristics this vector will undergo a change $l \rightarrow \widetilde{l}$. Assuming a linear model of light-camera interaction, Healey *et al* [3] considered that $\widetilde{l} = \mathbf{A} \cdot l$, where $\mathbf{A}$ is a $D \times D$ matrix. We may call this the *particular affine model*. In case $\mathbf{A}$ is restricted to be a diagonal matrix, we call it the *diagonal affine model*. On the other hand, a general affine transformation model could be motivated by the inclusion of effects like noise in the camera, or the *path radiance* term in Remote Sensing, and therefore $\widetilde{l} = \mathbf{B} \cdot l + t$, where $\mathbf{B}$ is also a $D \times D$ matrix. We call this the *general affine model*. The estimation of the $\mathbf{B}$ matrix and the t vector can be obtained adapting the method explained in [4] for the case of multispectral images. The $\mathbf{A}$ matrix can be obtained using the procedure explained in [5].

3. EXPERIMENTAL SETUP

3.1. Generation of a synthetic image

The generation of reliable ground-truth in relation to the application of image classification techniques of hyperspectral imagery is difficult and expensive in real scenarios. In order to avoid these problems, simulation of hyperspectral imagery (creation of synthetic images) is commonly used as a way to perform the evaluation of these classification techniques.

The synthetic image we used was created using a tool called *H-COMP* [6]. With *H-COMP* the user can interactively draw regions on the generated image, and associate spectral signatures from available libraries to each region. Random noise can also be added to the scenes to simulate contributions from ambient (clutter) and sensor sources.

The synthetic image is based on an atmospherically corrected image acquired by CHRIS-PROBA sensor of a test site in Barrax, 20 Km away from Albacete (Spain). The area is characterized by a flat morphology and large, uniform land-use units. Differences in elevation range up to 2m only.

After the *refectance synthetic image* is created, white noise (independent, identically distributed Gaussian process with zero mean and covariance matrix $\sigma^2\mathbf{I}$) is added to this image on each channel, with a Signal-To-Noise-ratio (SNR) equal to 10. In this case, SNR is defined as 50% reflectance divided by the standard deviation of the noise. In Figure 1 we can see a false colour image generated using 3 channels in the short, mid and long optical wavelength range, and a grey-colour image of 1 channel of the synthetic image with a white

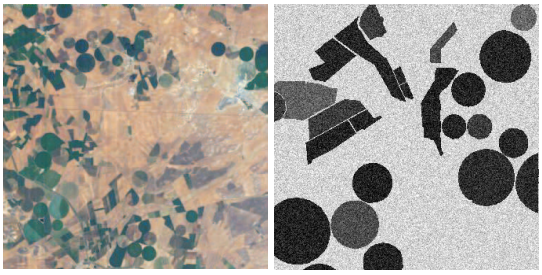

Fig. 1. (a) False colour RGB image of Barrax, (b) One of the channels of the synthetic image with SNR noise equal to 10.

noise added of $SNR = 10$. The noise-free synthetic image contains a series of land units (crop types) whose reflectance in the interval $[400, 1002]$ nm is obtained as the mean value of the reflectance for all the pixels of the same land unit for the atmospherically corrected CHRIS-PROBA image.

3.2. Evaluation of changes in the scattering characteristics of the atmosphere

In this paper, we are mainly interested in the evaluation of the compensation capability in terms of the change in the scattering properties of the atmosphere. These properties are mainly reflected in the $T \uparrow$ and $T \downarrow$ spectral curves. To isolate these changes from those of absorption, we apply a method called *peak stripping* but for absorption valleys. The original method by Clayton *et al* [7] compares the value of channel i with the mean of its 2 direct neighbours, i. e., $m_i = \frac{y_{(i-1)}+y_{(i+1)}}{2}$. If $y_i < m_i$ then $y_i \leftarrow m_i$, and otherwise left unchanged. In our case, the condition is if $y_i > m_i$ then $y_i \leftarrow m_i$. This process needs to be repeated on an iterative basis to obtain a reduction in these valleys. In Figure 2 we can see the result of the application of this *smoothing-like* algorithm to the curve $t_g \cdot T \uparrow$ for the typical atmospherical conditions of Barrax test site when CHRIS-PROBA satellite acquired the images on July the $16th$ 2004.

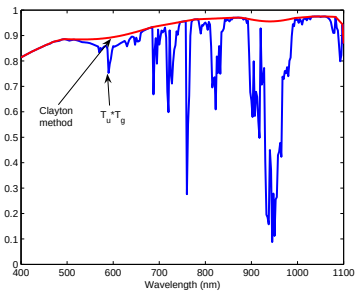

Fig. 2. $1000 - th$ iteration of the Clayton method on $t_g \cdot T \uparrow$.

3.3. Assessment of the compensation

Considering a point set in the form of a $N \times D$ matrix $\mathbf{X}$, where N is the number of points and D the dimension of the space where the points are, the *Frobenius matrix norm* is defined as $\|\mathbf{X}\|_F = \sqrt{\sum_{i=1}^{N}\sum_{j=1}^{D}|x_{ij}|^2}$ where x_{ij} is the element occupying the ith row and jth column in the matrix $\mathbf{X}$. For 2 $N \times D$ matrices ($\mathbf{A}$ and $\mathbf{B}$), and the compensation $\mathbf{B} \rightarrow \widetilde{\mathbf{B}}$, we could establish the following relative frobenius index as a measure of the illumination compensation performance: $F_I = \frac{\|\mathbf{A}-\widetilde{\mathbf{B}}\|_F}{\|\mathbf{A}\|_F}$

4. RESULTS AND DISCUSSION

In order to assess the application of the affine transformation models described in Section 2 in the case of a change in the scattering properties of the atmosphere we change the visibility parameter in the $6S$ code which directly affects the optical path and therefore is related to the scattering process.

Visibility is changed from 5.5 Km to 150 Km uniformly on the *log* scale, generating a group of 31 different values. We consider this variability for 3 different solar times, 7 AM, 12 and 16 PM. The 3 models of illumination compensation are compared for the change in visibility, considering the radiance image at $V = 5.5$ km as our *target image*.

$6S$ code needs a series of parameters to be introduced as input files that basically characterize the type of atmosphere to deal with. The parameters used here are representative and appropriate for the particular test site (i. .e, Barrax zone), because they are close to those directly obtained in Barrax during a campaign made in June and July 2004 [8]. The height of the region is fixed at 0.7 Km, O_3 (Ozone) content to 300 Dobson Units (DU) (i. e., 3 cm column) and the water vapour column at 2.5 cm. The atmospheric model selected is that called $US62$ in the $6S$ code, and the aerosol model type is the *Continental*. We require the maximum wavelength precision to the $6S$ code (2.5 nm). The zenith and azimuth coordinates of the sensor position are those obtained at 11AM solar time during the Barrax campaign on July the $16th$ 2004 [8], i. e., Zenith angle$= 8.80°$, Azimuth angle$= 224.28°$, which corresponds to a *Flight Zenith Angle* (FZA) of the CHRIS-PROBA satellite of $= 0°$.

Once the spectral distribution of the main variables in Eq. 1 are returned by the $6S$ code (i. e., t_g, $T\uparrow$, $T\downarrow$, S, L_0, and E_{sc}), the Clayton method is applied on the product $T\uparrow \cdot T\downarrow$ iteratively 1000 times for each one of them, for the different Visibility values and solar times, and then Eq. 1 is used to generate the corresponding radiance images.

A 5-*fold cross-validation* process [9] was applied on the pixels of the image to *validate* the 3 affine models.

In Figure 3 we can see the evolution of the F_I index for the 3 affine compensation models for the 3 solar times considered. It can be proved that the mean value of the relative

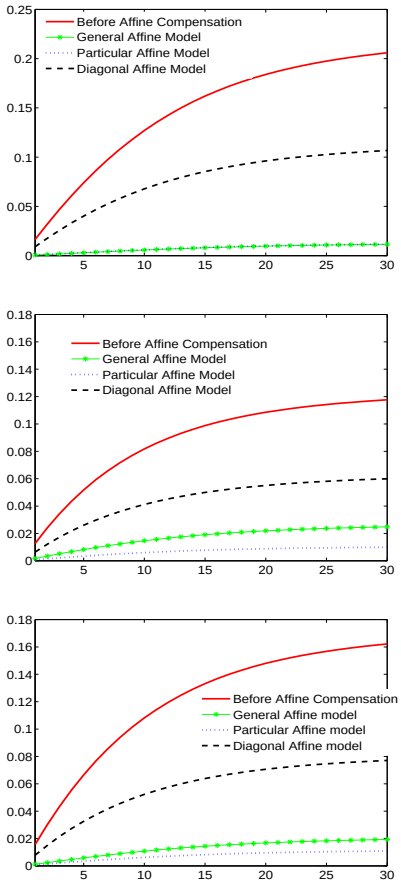

Fig. 3. F_I Index for (a) 7 AM. (b) 12 PM. (c) 16 PM.

Frobenius norm of the particular affine model is 2.8% higher than the mean value of the general affine model for 7AM. On the other hand, it can be proved that the mean value of the relative Frobenius norm of the general affine model is 74.80% higher than the mean value of the particular affine model for 16PM, and it is 146% higher than the mean value of the particular affine model for 12PM, and therefore the performance of the general affine model decreases from 16PM to 12PM.

The behaviour of the general affine model with respect to the particular affine model may be explained by the path radiance term and its variation with the change in visibility being higher for 7 AM, than for 12PM and 16PM. If this were the case, we would also foresee that the relevance of the *path radiance* term would be intermediate for 16 PM, in relation to 7 AM and 12PM (being the lowest for 12PM).

In order to analyze this hypothesis and establish the importance of the *path radiance* term for the 3 different *solar times* considered, let us define the following *merit number*

$$M_n = \frac{\int_{\lambda_{min}}^{\lambda_{max}} L_{path} d\lambda}{\int_{\lambda_{min}}^{\lambda_{max}} \overline{L_{surf}} d\lambda}, \qquad (2)$$

applicable to each one of the *visibility* and solar time values, where $\overline{L_{surf}}$ is the mean value of L_{surf} over the whole radiance image

$$\overline{L_{surf}} = \frac{1}{L_i L_j} \sum_{i=1}^{i=L_i} \sum_{j=1}^{i=L_j} L_{surf}(i,j) \quad (3)$$

Numerical integration in both cases is made using a piecewise linear interpolant [10]. This is because the centers of the filtering windows of CHRIS-PROBA sensor are not equally spaced. Following [10], let us consider the following integral

$$I = \int_{x_1}^{x_n} g(x)dx = \sum_{i=1}^{n-1} \int_{x_i}^{x_{i+1}} g(x)dx \quad (4)$$

where g is assumed to be linear between x_i and x_{i+1}. Therefore we may write

$$I = \frac{1}{2} \sum_{i=1}^{n-1} (x_{i+1} - x_i) \cdot (y_i + y_{i+1}) \quad (5)$$

where $y_i = g(x_i)$. In Figure 4 we can see that M_n is the highest for 7AM, for the whole visibility range, being the second 16PM, and 12PM the last one (this result supports our hypothesis). So the *path radiance* term is more important in *absolute terms* for 7AM than for the other two. It is also important to indicate that the slope in the curve for 7AM is higher (above all) for low visibility values, which supports the physics behind a general affine transformation model for 7AM, where an *offset* term exists. For the other 2 solar times, L_{path} contribution and variation are lower, therefore it may make sense to consider that a general affine model work worse than a particular affine model.

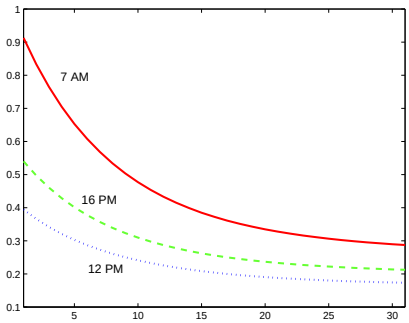

Fig. 4. M_n merit figure (Eq. 2) for different Visibility values and the 3 different solar times used.

5. CONCLUSIONS

In this paper we have shown that the affine model used by Heikkila *et al* in [4] can be used to compensate for illumination variations in radiance images due to changes in the scattering properties of the atmosphere. We have also assessed the performance of the particular and diagonal affine models, in all cases using a 5-fold cross-validation technique [9]. Experimental results showed that the diagonal affine model is the worst of the 3, while the particular model provided the best results, with the general affine model only better at the 7AM solar time. This strategy to compensate for illumination variability may be useful when huge amounts of multispectral images need to be processed in a short time interval.

Acknowledgments.

This work has been partially funded by the *EODIX* project ($AYA2008-05965-C04-04/ESP$), and the *MIPRCV* project ($CSD2007-00018$) The authors also thank Dr. Javier Plaza, from Universidad de Extremadura.

6. REFERENCES

[1] commission of the european communities, "Global monitoring for environment and security : 2004-2008," Tech. Rep., 2004.

[2] E. F. Vermote, D. Tanr, J. L. Deuze, M. Herman, and J. J. Morcrette, "Second simulation of the satellite signal in the solar spectrum: an overview," *IEEE TGARS*, vol. 35, pp. 675–686, 1997.

[3] C. Y. Kuan and G. Healey, "Retrieving multispectral satellite images using physics-based invariant representations," *IEEE Trans. PAMI*, vol. 18, pp. 842–848, 1996.

[4] J. Heikkila, "Pattern matching with affine moment descriptors," *Pattern Recognition*, vol. 37, pp. 1825–1834, 2004.

[5] G. D. Finlayson, M. S. Drew, and B. V. Funt, "Spectral sharpening: sensor transformations for improved color constancy," *JOSA-A*, vol. 11, pp. 1553–1563, 1994.

[6] J. Plaza, A. Plaza, P. Martinez, and R. Perez, "H-comp: A tool for quantitative and comparative analysis of endmember identification algorithms," in *IEEE IGARSS*, 2003, pp. 291–293.

[7] E. Clayton, P Duerden, and D. D. Cohen, "A discussion of pixan and pixanpc: The aaec pixe analysis computer packages," *Nucl. Instrum. Methods*, vol. B22, 1987.

[8] J. F. Moreno, "Sparc 2004 data acquisition report," Tech. Rep., Universidad de Valencia, 2004.

[9] R. E. Duda, P. E. Hart, and D. G. Stork, *Pattern Classification*, John Wiley & Sons, 2nd edition, 2000.

[10] D. Kahaner, C. Moler, and S. Nash, *Numerical methods and software*, Prentice Hall, 1989.